Broadband frequency conversion and shaping of single photons emitted from a nonlinear cavity

Murray W. McCutcheon[1†]**, Darrick E. Chang**[2†]**, Yinan Zhang**[1]**, Mikhail D. Lukin**[3]**, and Marko Lončar**[1]

[1]*School of Engineering and Applied Sciences, Harvard University, Cambridge, MA 02138*
[2]*Institute for Quantum Information and Center for the Physics of Information, California Institute of Technology, Pasadena, CA 91125*
[3]*Physics Department, Harvard University, Cambridge, MA 02138*
[†] *These authors contributed equally.*

murray@seas.harvard.edu

Abstract: Much recent effort has focused on coupling individual quantum emitters to optical microcavities in order to produce single photons on demand, enable single-photon optical switching, and implement functional nodes of a quantum network. Techniques to control the bandwidth and frequency of the outgoing single photons are of practical importance, allowing direct emission into telecommunications wavelengths and "hybrid" quantum networks incorporating different emitters. Here, we describe an integrated approach involving a quantum emitter coupled to a nonlinear optical resonator, in which the emission wavelength and pulse shape are controlled using the intra-cavity nonlinearity. Our scheme is general in nature, and demonstrates how the photonic environment of a quantum emitter can be tailored to determine the emission properties. As specific examples, we discuss a high Q-factor, TE-TM double-mode photonic crystal cavity design that allows for direct generation of single photons at telecom wavelengths (1425 nm) starting from an InAs/GaAs quantum dot with a 950 nm transition wavelength, and a scheme for direct optical coupling between such a quantum dot and a diamond nitrogen-vacancy center at 637 nm.

© 2009 Optical Society of America

OCIS codes: (270.5580) Quantum information processing; (230.5298) Photonic crystals; (230.5750) Resonators; (270.5580) Quantum electrodynamics

---

References and links

1. P. Michler, A. Kiraz, C. Becher, W. V. Schoenfeld, P. M. Petroff, L. Zhang, E. Hu, and A. Imamoglu, "A Quantum Dot Single-Photon Turnstile Device," Science **290**(5500), 2282–2285 (2000).
2. M. Pelton, C. Santori, J. Vučković, B. Zhang, G. S. Solomon, J. Plant, and Y. Yamamoto, "Efficient Source of Single Photons: A Single Quantum Dot in a Micropost Microcavity," Phys. Rev. Lett. **89**(23), 233602 (2002).
3. J. McKeever, A. Boca, A. D. Boozer, R. Miller, J. R. Buck, A. Kuzmich, and H. J. Kimble, "Deterministic Generation of Single Photons from One Atom Trapped in a Cavity," Science **303**(5666), 1992–1994 (2004).
4. L.-M. Duan and H. J. Kimble, "Scalable Photonic Quantum Computation through Cavity-Assisted Interactions," Phys. Rev. Lett. **92**(12), 127902 (2004).
5. K. M. Birnbaum, A. Boca, R. Miller, A. D. Boozer, T. E. Northup, and H. J. Kimble, "Photon blockade in an optical cavity with one trapped atom," Nature **436**, 87–90 (2005).

---

6. J. I. Cirac, P. Zoller, H. J. Kimble, and H. Mabuchi, "Quantum state transfer and entanglement distribution among distant nodes in a quantum network," Phys. Rev. Lett. **78**, 3221–3224 (1997).
7. H. J. Kimble, "The quantum internet," Nature **453**, 1023–1030 (2008).
8. M. V. Gurudev Dutt, L. Childress, L. Jiang, E. Togan, J. Maze, F. Jelezko, A. S. Zibrov, P. R. Hemmer, and M. D. Lukin, "Quantum register based on individual electronic and nuclear spin qubits in diamond," Science **316** 1312–1316 (2007).
9. C. Santori, P. Tamarat, P. Neumann, J. Wrachtrup, D. Fattal, R. G. Beausoleil, J. Rabeau, P. Olivero, A. D. Greentree, S. Prawer, F. Jelezko, and P. Hemmer, "Coherent population trapping of single spins in diamond under optical excitation," Phys. Rev. Lett. **97**, 247401 (2006).
10. T. Gaebel, M. Domhan, I. Popa, C. Wittmann, P. Neumann, F. Jelezko, J. R. Rabeau, N. Stavrias, A. D. Greentree, S. Prawer, J. Meijer, J. Twamley, P. R. Hemmer, and J. Wachtrup, "Room-temperature coherent coupling of single spins in diamond," Nature Phys. **2**, 408–413 (2006).
11. R. Hanson, F. M. Mendoza, R. J. Epstein, and D. D. Awschalom, "Polarization and readout of coupled single spins in diamond," Phys. Rev. Lett. **97**, 087601 (2006).
12. K. Srinivasan and O. Painter, "Linear and nonlinear optical spectroscopy of a strongly coupled microdisk-quantum dot system," Nature **450**, 862–865 (2007).
13. K. Hennessy, A. Badolato, M. Winger, D. Gerace, M. Atature, S. Gulde, S. Falt, E. L. Hu, and A. Imamoglu, "Quantum nature of a strongly coupled single quantum dot-cavity system," Nature, **445**, 896–899 (2007).
14. D. Englund, A. Faraon, I. Fushman, N. Stoltz, P. Petroff, and J. Vučković, "Controlling cavity reflectivity with a single quantum dot," Nature, **450**, 857–861 (2007).
15. D. F. Phillips, A. Fleischhauer, A. Mair, R. L. Walsworth, and M. D. Lukin, "Storage of Light in Atomic Vapor," Phys. Rev. Lett. **86**(5), 783–786 (2001).
16. C. Liu, Z. Dutton, C. H. Behroozi, and L. V. Hau, "Observation of coherent optical information storage in an atomic medium using stored light pulses," Nature **409**, 490–493 (2001).
17. Y. Zhang, M. W. McCutcheon, I. B. Burgess, and M. Lončar, "Ultra-high-Q TE/TM dual-polarized photonic crystal nanocavities," Opt. Lett. **34**, 2694–2696 (2009).
18. M. W. McCutcheon, J. F. Young, G. W. Rieger, D. Dalacu, S. Frédérick, P. J. Poole, and R. L. Williams, "Experimental demonstration of second-order processes in photonic crystal microcavities at submilliwatt excitation powers," Phys. Rev. B **76**, 245104 (2007).
19. A. Rodriguez, M. Soljacic, J. D. Joannopoulos, and S. G. Johnson, "$\chi^{(2)}$ and $\chi^{(3)}$ harmonic generation at a critical power in inhomogeneous doubly resonant cavities," Opt. Express **15**, 7303–7318 (2007).
20. J. Bravo-Abad, A. Rodriguez, P. Bermel, S. G. Johnson, J. D. Joannopoulos, and M. Soljacic, "Enhanced nonlinear optics in photonic-crystal microcavities," Opt. Express **15**, 16161–16176 (2007).
21. M. Liscidini and L. C. Andreani, "Second-harmonic generation in doubly resonant microcavities with periodic dielectric mirrors," Phys. Rev. E **73**, 016613 (2006).
22. A. R. Cowan and J. F. Young, "Nonlinear optics in high refractive index contrast periodic structures," Semicond. Sci. Technol. **20**, R41–R56 (2005).
23. M. W. McCutcheon, G. W. Rieger, J. F. Young, D. Dalacu, P. J. Poole, and R. L. Williams, "All-optical conditional logic with a nonlinear photonic crystal nanocavity," Appl. Phys. Lett. **95**, (2009).
24. R. W. Boyd, *Nonlinear Optics* (Academic, New York, 1992).
25. M. D. Eisaman, A. André, F. Massou, M. Fleischhauer, A. S. Zibrov, and M. D. Lukin, "Electromagnetically induced transparency with tunable single-photon pulses," Nature **438**, 837–841 (2005.)
26. A. P. VanDevender and P. G. Kwiat, "High efficiency single photon detection via frequency up-conversion," J. Mod. Opt. **51**, 1433–1445 (2004).
27. C. Langrock, E. Diamanti, R. V. Roussev, Y. Yamamoto, M. M. Fejer, and H. Takesue, "Highly efficient single-photon detection at communication wavelengths by use of upconversion in reverse-proton-exchanged periodically poled linbo3 waveguides," Opt. Lett. **30**(13), 1725–1727 (2005).
28. S. Tanzilli, W. Tittel, M. Halder, O. Alibart, P. Baldi, N. Gisin, and H. Zbinden, "A photonic quantum information interface," Nature **437** 116–120 (2005).
29. A. P. VanDevender and P. G. Kwiat, "Quantum transduction via frequency upconversion (invited)," J. Opt. Soc. Am. B **24**(2), 295–299 (2007).
30. X. Xu, B. Sun, P. R. Berman, D. G. Steel, A. S. Bracker, D. Gammon, and L. J. Sham, "Coherent population trapping of an electron spin in a single negatively charged quantum dot," Nature Phys. **4**, 692–695 (2008).
31. A. V. Gorshkov, A. A., M. Fleischhauer, A. S. Sørensen, and M. D. Lukin, "Universal approach to optimal photon storage in atomic media," Phys. Rev. Lett. **98**(12), 123601 (2007).
32. T. Tanabe, M. Notomi, A. Mitsugi, A. Shinya, and E. Kuramochi, "All-optical switches on a silicon chip realized using photonic crystal nanocavities," Appl. Phys. Lett. **87**, 151112 (2005).
33. S. Combrié, A. De Rossi, Q. V. Tran, and H. Benisty, "GaAs photonic crystal cavity with ultrahigh Q: microwatt nonlinearity at 1.55 μm," Opt. Lett. **33**, 1908–1910 (2008).
34. R. Herrmann, T. S unner, T. Hein, A. L offler, M. Kamp, and A. Forchel, "Ultrahigh-quality photonic crystal cavity in GaAs," Opt. Lett. **31**, 1229–1231 (2006).
35. C. Sauvan, G. Lecamp, P. Lalanne, and J. P. Hugonin, "Modal-reflectivity enhancement by geometry tuning in

photonic crystal microcavities," Opt. Express **13**, 245–255 (2005).

36. A. R. M. Zain, N. P. Johnson, M. Sorel, and R. M. De la Rue, "Ultra high Quality factor one dimensional photonic crystal/photonic wire micro-cavities in silicon-on-insulator (SOI)," Opt. Express **16**, 12084–12089 (2008).

37. M. W. McCutcheon and M. Lončar, "Design of a silicon nitride photonic crystal nanocavity with a Quality factor of one million for coupling to a diamond nanocrystal," Opt. Express **16**, 19136–19145 (2008).

38. M. Notomi, E. Kuramochi, and H. Taniyama, "Ultrahigh-Q nanocavity with 1D photonic gap," Opt. Express **16**, 11095–11102 (2008).

39. J. Chan, M. Eichenfield, R. Camacho, and O. Painter, "Optical and mechanical design of a "zipper" photonic crystal optomechanical cavity," Opt. Express **17**, 3802–3817 (2009).

40. P. B. Deotare, M. W. McCutcheon, I. W. Frank, M. Khan, and M. Lončar, "High quality factor photonic crystal nanobeam cavities," Appl. Phys. Lett. **94**, 121106 (2009).

41. M. L. Povinelli, M. Lončar, M. Ibanescu, E. J. Smythe, S. G. Johnson, F. Capasso, and J. D. Joannopoulos, "Evanescent-wave bonding between optical waveguides," Opt. Lett. **30**, 3042–3044 (2005).

42. M. Eichenfield, R. Camacho, J. Chan, K. J. Vahala, and O. Painter, "A picogram and nanometer scale photonic crystal opto-mechanical cavity," Nature **459**, 550–556 (2009).

43. M. E. Reimer, D. Dalacu, J. Lapointe, P. J. Poole, D. Kim, G. C. Aers, W. R. McKinnon, and R. L. Williams, "Single electron charging in deterministically positioned InAs/InP quantum dots," Appl. Phys. Lett. **94**, 011108 (2009).

44. E. H. Sargent, "Infrared quantum dots," Adv. Mat. **17** 515–522 (2005).

45. M. B. Ward, T. Farrow, P. See, Z. L. Yuan, O. Z. Karimov, A. J. Bennett, A. J. Shields, P. Atkinson, K. Cooper, and D. A. Ritchie, "Electrically driven telecommunication wavelength single-photon source," Appl. Phys. Lett. **90**, 063512 (2007).

46. T. Miyazawa, S. Okumura, S. Hirose, K. Takemoto, M. Takatsu, T. Usuki, N. Yokoyama, and Y. Arakawa, "First demonstration of electrically driven 1.55 μm single-photon generator," Jap. J. Appl. Phys. **47** 2880–2883 (2008).

47. E. D. Palik, *Handbook of optical constants of solids Vol. 1.* (Academic Press, Inc., 1985).

48. , *Handbook of laser science and technology, Vol. III: Optical Materials, Part I*, chapter Non-linear optical materials, (CRC Press, 1986).

49. I. Shoji, T. Kondo, A. Kitamoto, M. Shirane, and R. Ito, "Absolute scale of second-order nonlinear-optical coefficients," J. Opt. Soc. Am. B **14**, 2268–2294 (1997).

50. R. C. Stoneman and L. Esterowitz, "Efficient resonantly pumped 2.8-μm er^{3+}:gsgg laser," Opt. Lett. **17**, 816–818 (1992).

51. C. Kurtsiefer, S. Mayer, P. Zarda, and H. Weinfurter, "Stable solid-state source of single photons," Phys. Rev. Lett. **85**, 290–293 (2000).

52. C. F. Wang, R. Hanson, D. D. Awschalom, E. L. Hu, T. Feygelson, J. Yang, and J. E. Butler, "Fabrication and characterization of two-dimensional photonic crystal microcavities in nanocrystalline diamond," Appl. Phys. Lett. **91**, 201112 (2007).

53. P. E. Barclay, K.-M. C. Fu, C. Santori, and R. G. Beausoleil, "Chip-based microcavities coupled to nitrogen-vacancy centers in single crystal diamond," Appl. Phys. Lett. **95**, 191115 (2009).

54. P. E. Barclay, K.-M. C. Fu, C. Santori, and R. G. Beausoleil, "Hybrid photonic crystal cavity and waveguide for coupling to diamond NV-centers," Opt. Express **17**, 9588–9601 (2009).

55. K.-M. C. Fu, C. Santori, P. E. Barclay, I. Aharonovich, S. Prawer, N. Meyer, A. M. Holm, and R. G. Beausoleil, "Coupling of nitrogen-vacancy centers in diamond to a GaP waveguide," Appl. Phys. Lett. **93**, 234107 (2008).

56. K. Rivoire, A. Faraon, and J. Vučković, "Gallium phosphide photonic crystal nanocavities in the visible," Appl. Phys. Lett. **93**, 063103 (2008).

57. P. E. Barclay, C. Santori, K.-M. C. Fu, R. G. Beausoleil, and O. Painter, "Coherent interference effects in a nano-assembled diamond NV center cavity-QED system," Opt. Express **17**, 8081–8097 (2009).

58. M. Barth, N. Nusse, B. Lochel, and O. Benson, "Controlled coupling of a single-diamond nanocrystal to a photonic crystal cavity," Opt. Lett. **34**, 1108–1110 (2009).

59. P. B. Deotare, M. W. McCutcheon, I. W. Frank, M. Khan, and M. Lončar, "Coupled photonic crystal nanobeam cavities," Appl. Phys. Lett. **95**, 031102 (2009).

60. I. W. Frank, P. B. Deotare, M. W. McCutcheon, and M. Lončar, "Dynamically reconfigurable photonic crystal nanobeam cavities," arxiv:0909.2278v1 Phys. Opt. (2009).

61. P. E. Barclay, K. Srinivasan, O. Painter, B. Lev, and H. Mabuchi, "Integration of fiber-coupled high-Q SiN$_x$ microdisks with atom chips," Appl. Phys. Lett. **13**, 801 (2005).

62. C. Cabrillo, J. I. Cirac, P. García-Fernández, and P. Zoller, "Creation of entangled states of distant atoms by interference," Phys. Rev. A **59**(2), 1025–1033 (1999).

63. S. Bose, P. L. Knight, M. B. Plenio, and V. Vedral, "Proposal for Teleportation of an Atomic State via Cavity Decay," Phys. Rev. Lett. **83**, 24 5158–5161 (1999).

64. L.-M. Duan and H. J. Kimble, "Efficient Engineering of Multiatom Entanglement through Single-Photon Detections," Phys. Rev. Lett. **90**(25), 253601 (2003).

65. A. K. Ekert, "Quantum cryptography based on Bell's theorem," Phys. Rev. Lett. **67**(6), 661–663 (1991).

66. M. O. Scully and M. S. Zubairy, *Quantum Optics* (Cambridge University Press, Cambridge, UK 1997).

1. Introduction

In recent years, there has been a concerted research effort towards achieving strong coupling between single quantum emitters and high-finesse, resonant optical microcavities (cavity QED) [1, 2, 3]. The strong coupling results in preferential emission into the cavity mode of a single photon with frequency near the emitter resonance. This is beneficial to generate single photons on demand, realize large optical nonlinearities at a single-photon level [4, 5] for low-power switching or quantum logic gates, and facilitate communication between distant nodes of a quantum network [6, 7]. In state-of-the-art systems, however, the operating (emission) wavelength is determined by the material properties of the quantum emitter – namely, the atomic or excitonic resonance frequency. With the exception of quantum dots, this wavelength is *fixed* and *cannot be engineered*. For example, the operating wavelength of systems based on Cs or Rb atoms is limited to 852 nm and 780 nm, respectively. In practice, however, the ability to substantially shift the emission frequency would open up a number of important possibilities, including direct emission into low-loss telecom frequency bands for long-distance transmission of photons over existing communication channels. It would also allow direct coupling between different types of emitters, enabling hybrid quantum networks in which the best attributes of various emitters can be combined – *e.g.*, allowing single photons generated by solid-state systems [8, 9, 10, 11, 12, 13, 14] to be coherently stored for long times in atomic gases [15, 16]. This would be an important step towards realizing fully functional quantum networks (with sources, processors, memory, etc.). Similarly, tailoring the bandwidth of the emitted photons would allow for fast communication and operation times.

Here, we demonstrate a novel approach to achieve these goals based on a quantum emitter strongly coupled to a nonlinear optical resonator, where the optical emission is directly frequency-shifted into the desired domain using efficient intracavity nonlinear optical processes. By tailoring the optical degrees of freedom (resonances) of such a system, we demonstrate that the wavelength of the emitted photons can be shifted over a large spectral range (more than 500 nm) with high efficiency. Our approach allows direct control of the single photon shape and bandwidth, which is important for efficient and rapid optical coupling between quantum nodes [6]. As a practical implementation, we propose a system based on a doubly resonant nonlinear photonic crystal cavity [17] which allows for up to ∼ 99% photon conversion efficiencies. This system facilitates nonlinear optical processes at a wavelength scale, and is therefore of interest for the realization of integrated platforms that can operate at low power levels [18, 19, 20, 21, 22, 23]. Moreover, our system allows for the integration of large arrays of single-photon sources, each tailored to emit at different wavelengths (within the ∼500 nm wide wavelength range) using *the same type* of quantum emitter. This could facilitate the realization of multi-color single-photon sources which could be used for secure optical interconnects.

Our technique is quite robust in that the maximum efficiency does not depend on an explicit phase-matching condition [24], as would occur in an extended nonlinear crystal, but rather only on the ratio of the cavity Quality factor to mode volume (Q/V). This figure of merit can be extremely high in realistic photonic crystal structures. As an example, we demonstrate a novel double mode TE-TM cavity design in a GaAs photonic crystal that is well-suited for the conversion of photons from the near infrared to the telecom band. We also present a similar GaP-based design suitable for direct coupling between a nitrogen-vacancy center in diamond [8, 9, 10, 11] and an InAs/GaAs quantum dot [12, 13, 14], which could enable practical realization of a hybrid quantum network.

Finally, we emphasize that our proposal has a number of advantages compared to previous schemes for spectral control of single photons [25, 26, 27, 28, 29], in that here one can *simultaneously* shift the emission wavelength over hundreds of nm and enhance the emission bandwidth on an integrated platform. In contrast, techniques based on electromagnetically in-

duced transparency in atomic vapors [25] cannot enhance the photon bandwidth over the atomic linewidth, and wavelength tailoring is practical only very near the atomic resonant wavelength where the atoms have a significant optical response ($\lesssim$ 1 nm tuning range). On the other hand, macroscopic nonlinear crystals have been used to achieve wavelength conversion over hundreds of nm [26, 27, 28, 29], but these approaches offer no bandwidth control and require separate single-photon sources as inputs. Moreover, they require stringent phase-matching conditions and high peak-power laser pulses for efficient conversion. Our nanophotonics platform overcomes these shortcomings, thereby enabling highly efficient conversion and bandwidth control of single photons in mode volumes smaller than a cubic wavelength.

2. The concept of single-photon spectral control

We first discuss the general protocol for generating single photons on demand at arbitrary frequencies using a nonlinear double-mode cavity, and introduce a simple theoretical model to derive the efficiency of the process. The system of interest is illustrated schematically in Fig. 1. As in standard cavity-based single-photon generation protocols [6, 3], a single three-level atom (or any other quantum dipole emitter) is resonantly coupled to one mode (here denoted a) of an optical cavity. The emitter is initialized through optical pumping in state $|s\rangle$, the specific nature of which depends on the type of emitter used. This is a standard technique for preparing the initial state of an emitter, and has been experimentally demonstrated for both quantum dots [30] and diamond NV centers [9]. An external laser field with controllable Rabi frequency $\Omega(t)$ couples $|s\rangle$ to excited state $|e\rangle$. The transition between $|e\rangle$ and ground state $|g\rangle$ is resonantly coupled to cavity mode a (frequency ω_a), with a single-photon Rabi frequency g_1. The relevant decay mechanisms (illustrated with gray arrows in the figure) are a leakage rate κ_a for photons to leave cavity mode a, and a rate γ that $|e\rangle$ spontaneously emits into free space rather than into the cavity. Conventionally, in absence of an optical nonlinearity, the control field $\Omega(t)$ creates a single atomic excitation at some desired time in the system, which via the coupling g_1 is converted into a single, resonant cavity photon. This photon eventually leaks out of the cavity and constitutes an outgoing, resonant single photon generated on demand whose spatial wave-packet can be shaped by properly choosing $\Omega(t)$ [6].

In our system, the cavity is also assumed to possess a second mode c with frequency ω_c, and our goal is to induce the single photon to exit at this frequency rather than ω_a. This can be achieved, provided that the cavity medium itself possesses a second-order ($\chi^{(2)}$) nonlinear susceptibility, by applying a classical pump field to the system at the difference frequency $\omega_b = \omega_a - \omega_c$. The induced coherent coupling rate between modes a and c is denoted g_2. The field b need not correspond to a cavity mode. Mode c has a photon leakage rate, which we separate into an "inherent" rate, $\kappa_{c,in}$, and a "desirable" (extrinsic) rate, $\kappa_{c,ex}$. $\kappa_{c,in}$ characterizes the natural leakage into radiation modes and also absorption losses, and can be expressed in terms of the (unloaded) cavity quality factor as $\kappa_{c,in} = \omega_c/2Q_c$. $\kappa_{c,ex}$ characterizes the outcoupling rate into any external waveguide used for photon extraction. The total leakage of mode c is then $\kappa_c = \kappa_{c,in} + \kappa_{c,ex}$.

More quantitatively, the effective Hamiltonian for the system (in a rotating frame) is given by

$$
\begin{aligned}
H_I &= H_c + H_{loss}, \\
H_c &= \hbar g_1(\sigma_{eg}a_a + \sigma_{ge}a_a^\dagger) + \hbar\Omega(t)(\sigma_{es} + \sigma_{se}) + \hbar g_2(a_a^\dagger a_c + a_a a_c^\dagger), \\
H_{loss} &= -\frac{i\gamma}{2}\sigma_{ee} - \frac{i\kappa_a}{2}a_a^\dagger a_a - \frac{i(\kappa_{c,ex} + \kappa_{c,in})}{2}a_c^\dagger a_c,
\end{aligned}
\tag{1}
$$

where H_c describes the coherent part of the system evolution (for simplicity we take $g_{1,2}, \Omega$ to be real), and H_{loss} is a non-Hermitian term characterizing the losses. $\sigma_{ij} = |i\rangle\langle j|$ are atomic

operators, while a_i is the photon annihilation operator for mode i. The vacuum Rabi splitting g_1 can be written in the form $g_1 = \mathbf{d} \cdot \mathbf{E}_a(\mathbf{r})/\hbar$, where $\mathbf{d}$ is the dipole matrix element of the $|g\rangle$-$|e\rangle$ transition, and $\mathbf{E}_a(\mathbf{r})$ is the electric field amplitude per photon at the emitter position $\mathbf{r}$. The electric field per photon in mode $i = a, c$ is determined by the normalization

$$\frac{\hbar \omega_i}{2} = \int d\mathbf{r} \varepsilon_0 \varepsilon(\mathbf{r}) |\mathbf{E}_i(\mathbf{r})|^2, \tag{2}$$

where $\varepsilon(\mathbf{r})$ is the dimensionless electric permittivity of the material. The nonlinearity parameter is given by [19]

$$g_2 = -\frac{\varepsilon_0}{\hbar} \int d\mathbf{r} \chi_{ijk}^{(2)} E_{a,i}^* \left(E_{b,j} E_{c,k} + E_{c,j} E_{b,k} \right). \tag{3}$$

The amplitudes $E_{a,c}$ appearing above are normalized by Eq. (2), while E_b is the classical pump amplitude. Importantly, one can compensate for a small nonlinear susceptibility $\chi^{(2)}$ or field overlap (phase matching) simply by using larger pump amplitudes E_b to achieve a desired g_2 strength.

For a system initialized in $|s\rangle$, there can never be more than one excitation, and the system generally exists as a superposition of having the system in state $|s\rangle$ or $|e\rangle$ (with no photons) or having a photon in one of the modes a, c (and the emitter in $|g\rangle$),

$$|\psi(t)\rangle = c_s(t)|s\rangle + c_e(t)|e\rangle + c_a(t)|1_a\rangle + c_c(t)|1_c\rangle. \tag{4}$$

The system is initialized to $c_s(0) = 1$ with all other $c_i(0) = 0$ and the time evolution is given by $\dot{c}_j = -(i/\hbar)\langle j|H_I|\psi(t)\rangle$. In this effective wave-function approach, provided that $|s\rangle$ is always
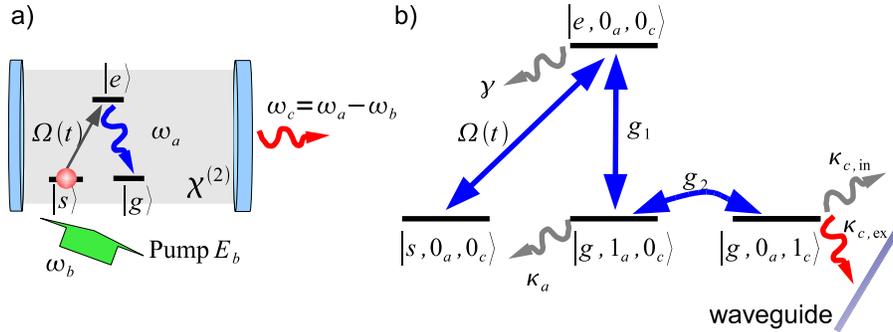

Fig. 1. Schematic of single-photon frequency conversion. a) A single three-level emitter is coupled to a double-mode cavity that possesses a $\chi^{(2)}$ nonlinearity. After excitation, the emitter emits a photon into the cavity at frequency ω_a. When the cavity is irradiated by the pump beam at ω_b, the photon is converted to a second cavity mode at frequency ω_c. b) Level diagram: coherent coupling strengths are indicated with blue arrows, while gray arrows denote undesirable loss mechanisms. The emitter is controllably pumped from initial state $|s\rangle$ via an external laser field $\Omega(t)$ to excited state $|e\rangle$. The excited state $|e\rangle$ can reversibly emit a single photon into cavity mode a (while bringing the atom into state $|g\rangle$) at a rate g_1, and can also decay into free space at rate γ. Mode a has an inherent decay rate given by κ_a. The nonlinearity allows the photon in mode a to be converted to one in mode c at a rate g_2 when the cavity is pumped by a laser of frequency $\omega_b = \omega_a - \omega_c$. The leakage rate of the frequency-converted photon at ω_c is split up into undesirable channels ($\kappa_{c,in}$) and desirable out-coupling to a nearby waveguide ($\kappa_{c,ex}$).

driven, $\sum_j |c_j|^2 \to 0$ as $t \to \infty$ due to losses, which can be connected with population leakage out of one of the aforementioned decay channels. In the limit that $\Omega(t)$ is small and varies slowly, all other $c_i(t)$ adiabatically follow $c_s(t)$ (see Appendix), and one finds

$$\dot{c}_e(t) \approx -i\Omega(t)c_s(t) - \frac{1}{2}\left(\gamma + \frac{4g_1^2}{\kappa_a + 4g_2^2/\kappa_c}\right)c_e. \qquad (5)$$

Physically, we can identify $\gamma_{total} = \gamma + \frac{4g_1^2}{\kappa_a + 4g_2^2/\kappa_c}$ as the cavity-enhanced total decay rate of $|e\rangle$, where the first (second) term corresponds to direct radiative emission (emission into mode a). Similarly, the denominator $\kappa_a + 4g_2^2/\kappa_c$ corresponds to the new total decay rate of mode a in the presence of an optical nonlinearity, as it yields a new channel for photons to effectively "decay" out of mode a into c at rate $4g_2^2/\kappa_c$. It is clear that some optimal value of g_2 exists for frequency conversion to occur. In particular, for no nonlinearity ($g_2 = 0$) this probability is non-existent. On the other hand, for $g_2 \to \infty$, one finds $\gamma_{total} = \gamma$, which indicates that the leakage from mode a into c is so strong that no cavity-enhanced emission occurs. Note that the use of a time-varying control field allows for arbitrary shaping of the outgoing single-photon wavepacket at frequency ω_c, provided only that the photon bandwidth is smaller than κ_c (physically, the photon cannot leave faster than the rate determined by the cavity decay; see Appendix). This feature is particularly useful in two respects. First, in practice κ_c can be much larger than γ, which enables extremely fast operation times. Second, pulse shaping is useful for constructing quantum networks, as it allows one to impedance-match the outgoing photon to other nodes of the network.

Based on the above arguments, the probability that a single photon of frequency ω_c is produced and extracted into the desired out-coupling waveguide is given by

$$F = \frac{C_{in}}{1 + \phi + C_{in}} \frac{\phi}{1 + \phi} \frac{\kappa_{c,ex}}{\kappa_c}, \qquad (6)$$

where $\phi = 4g_2^2/(\kappa_a \kappa_c)$ characterizes the branching ratio in mode a of nonlinearity-induced leakage to inherent losses, and $C_{in} = 4g_1^2/\gamma\kappa_a$ is the inherent cavity cooperativity parameter for mode a in absence of nonlinearity. The first term on the right denotes the probability for $|e\rangle$ to decay into mode a, the second term the probability that a photon in mode a couples into mode c, and the third term the probability that a photon in mode c out-couples into the desired channel (see Appendix for an exact calculation). ϕ depends on the pump amplitude E_b, with the optimal value $\phi = \sqrt{1 + C_{in}}$ yielding the maximum in F. For large $C_{in} \gg 1$, the maximum probability is

$$F \approx \left(1 - \frac{2}{\sqrt{C_{in}}}\right)\frac{\kappa_{c,ex}}{\kappa_c}. \qquad (7)$$

Considering an emitter placed near the field maximum of mode a, $C_{in} \sim \frac{3Q_a}{2\pi^2}\frac{\lambda_a^3}{n_a^3 V_a}\frac{\gamma_0}{\gamma}$, where Q_a, V_a are the mode quality factor and volume, respectively, and n is the index of refraction at frequency ω_a. The ratio γ/γ_0 is the spontaneous emission rate into non-cavity modes normalized by the spontaneous emission rate $\gamma_0 \equiv n\omega_a^3|\mathbf{d}|^2/(3\pi\varepsilon_0\hbar c^3)$ of an emitter embedded in an isotropic medium of index n. This ratio is expected to be of order $0.1 - 1$ for our devices of interest, and thus the efficiency essentially depends only on Q_a/V_a.

We have analyzed here the case of a purely radiative emitter. For certain solid-state emitters, dephasing of its electronic transitions may not be negligible. In the presence of dephasing, it is necessary to solve for the full density matrix ρ of the system (see Appendix). This yields a modified expression for the probability of frequency conversion (eq. (21)). However, we note that the effects of dephasing are likely to be small. For example, in the charged InAs quantum

dot in ref. [30], the dephasing rate is $\gamma_d = 0.54$ GHz, and in ref. [12], $\gamma_d = 1.17$ GHz. In the specific example we consider in Section 4, the effect of these decoherence channels on the frequency conversion probability (Fig. 3) is negligible. By the same token, in diamond NV centers, the dephasing rate of the electron spin can be extremely small, on the order of ~ 1 MHz [8].

Finally, while we have focused on the case of single-photon generation here, the reverse process can also be considered, where a single incoming photon at frequency ω_c is incident upon the system, converted into a photon in mode a, and coherently absorbed by an atom with the aid of an impedance-matched pulse $\Omega(t)$, causing its internal state to flip from $|g\rangle$ to $|s\rangle$. Generally, by time-reversal arguments [31], it can be shown that the probability F for single-photon storage is the same as that for generation.

3. Realization in a nonlinear photonic crystal cavity

In order to implement this frequency conversion scheme in a practical fashion, there are several constraints on the design of the cavity modes. For the nonlinear process to be efficient, mode a must have a high cooperativity (Q/V) to ensure strong coupling of the emitter (see Fig. 1). For mode c, a high Q factor (small κ_c) is important to maximize the nonlinear coupling parameter, ϕ, and hence reduce the pump power needed in order to reach the optimum nonlinear coupling strength, g_2. The cavity should also be composed of a $\chi^{(2)}$ nonlinear material that is transparent in the desired frequency range. Finally, in order for the modes to couple efficiently via the nonlinear susceptibility of the cavity, they must have a large spatial overlap and the appropriate vector orientation, as determined by the elements of the $\chi^{(2)}$ tensor of the cavity material (see Eq. (3)).

As a host platform for the nonlinear cavity, the III-V semiconductors are promising candidates because of their significant second-order nonlinear susceptibilities and mature nanofabrication technologies. However, the symmetry of the III-V group $\chi^{(2)}$ tensor ($\chi^{(2)}_{ijk} \neq 0, i \neq j \neq k$) requires that the dominant field components of the modes be orthogonal in order to maximize the nonlinear coupling. It further implies that if the classical field which drives the nonlinear polarization is incident from the normal direction (*e.g.*, from an off-chip laser), one of the cavity modes must have a TM polarization.

We adopt a photonic crystal platform to realize a wavelength-scale nonlinear cavity that meets these requirements. Recently, 2D photonic crystal nanocavities have shown great promise for strongly coupling an optical mode to a quantum dot emitter [13, 14]. In addition, they have been used as platforms for classical nonlinear optical generation and switching [18, 32]. Photonic crystal cavities with Q factors of up to 700,000 have been realized in GaAs [33, 34], which shows the feasibility of using a III-V platform for our proposal. The challenge, however, is to design a nonlinear photonic crystal nanocavity which supports two orthogonal, high cooperativity modes with a large mode field overlap.

To enable a monolithic cavity design which supports *both* TE *and* TM modes, we design a photonic crystal "nanobeam" cavity – a free-standing ridge waveguide patterned with a one-dimensional (1D) lattice of holes – for which we can control both TE and TM photonic bandstructures. Recently, there has been much interest in photonic crystal nanobeam cavities [35, 36, 37, 38, 39, 40] due to their exceptional cavity figures of merit (Q and V), relative ease of design and fabrication, and potential as a platform to realize novel optomechanical effects [41, 42]. Our frequency conversion scheme can be realized in a similar structure, as shown in Fig. 2. We optimize two high cooperativity cavity modes by exploiting the different quasi-1D TE and TM photonic stopbands of the patterned nanobeam (shaded regions in the inset of Fig. 2). A key design point is that the TE and TM bandstructures can be tuned somewhat independently by varying the cross-sectional aspect ratio of the ridge. For example, in a nanobeam
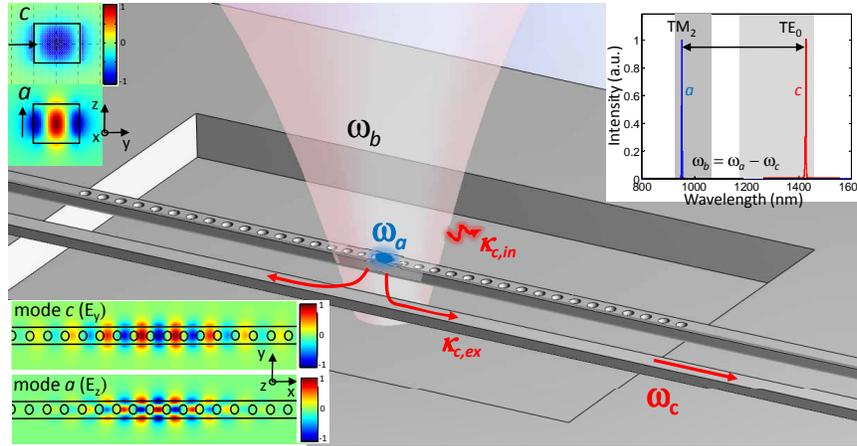
Fig. 2. Cavity mode characteristics. Frequency conversion platform based on a photonic crystal nanobeam cavity, integrated extraction waveguide, and off-chip coupling laser (ω_b) tuned to the difference frequency of the modes. The cavity is formed by introducing a local perturbation into a periodic 1D line of air holes in the free-standing nanobeam. The desirable ($\kappa_{c,ex}$) and inherent ($\kappa_{c,in}$) loss channels from mode c are shown. The insets show the schematic cavity spectrum with photonic stopbands shown in grey, and the dominant field components of the TE$_0$ (ω_c) and TM$_2$ (ω_a) modes. The yz-plane cross-sections of the modes (upper left) show the E_y (E_z) component of mode c (a) at the center of the cavity, highlighting the mode overlap and polarizations. In the optimized structure, the TE mode at 1425 nm has $Q = 1.4 \times 10^7$ and $V_n = 0.77$, and the TM mode at 950 nm has $Q = 1.3 \times 10^5$ and $V_n = 1.44$ (V_n is the mode volume normalized by $(\lambda/n)^3$). The inherent peak cooperativities for the modes are $C_{in}^{TE} = 2.4 \times 10^7$ and $C_{in}^{TM} = 3.7 \times 10^4$, which are well into the strong coupling regime, as given by $C > 1$.

with a square cross-section, the two stopbands overlap completely. As the width-to-depth ratio of the waveguide is increased, the effective index of the TE modes increases relative to the TM modes, shifting the TE stopband to longer wavelengths [17].

4. Example implementations

Although our scheme is general in nature, and does not depend on the particular flavor of emitter or wavelength of operation, it is interesting and instructive to consider some concrete examples. As a first example, we design a GaAs photonic crystal nanobeam cavity with modes at 950 nm and 1425 nm, which would be suitable for directly generating single photons at telecom wavelengths from InAs/GaAs quantum dots designed to emit near 950 nm. We note that quantum dots emitting near 1.5 μm do exist [43, 44], as do protocols for generating single photons at this wavelength [45, 46]. However, this example shows how "top-down" engineering of the photonic environment of a given emitter can completely determine its emission properties. In a solid-state system, this gives a great deal of flexibility in tailoring the emission frequency, avoiding the complexities of changing material systems, and paving the way for multiple devices with different operating frequencies on a single platform. Moreover, this approach is particularly powerful for atomic emitters, which are fixed in their emission frequency.

To achieve such a large spectral separation (950 – 1425 nm), we couple the fundamental TE$_0$ cavity mode to a *higher-order* TM$_2$ cavity mode (see inset Fig. 2). Crucially, the photonic crystal lattice tapering [37, 38, 39] is effective in enhancing the Q-factors of *both TE and TM modes*. The choice of 1425 nm was dictated by the constraint of maintaining a high Q-factor

($> 10^5$) for each mode. At wavelengths longer than 1425 nm, the TM$_2$ mode Q factor declines rapidly. We emphasize that this example is purely illustrative, and the quantum dot photon could be converted to any wavelength between 950 and 1425 nm with a suitable adjustment of the cavity geometry, provided a coupling laser with wavelength to match the modes' difference frequency was readily available.

The nanobeam cavities are formed by a 4-period taper in the size and spacing of the holes in the uniform photonic "mirror" on both sides of the cavity center in order to introduce a localized potential for the TE and TM modes. We assume the nanobeam is oriented such that the x and y directions as defined in Fig. 2 are commensurate with the [100] and [010] crystal axes of the GaAs. The 950-1425 nm cavity nanobeam has width $w = 389$ nm and depth $d = 285$ nm, and the hole spacing tapers from $a_0 = 334$ nm in the mirror to $a_c = 312$ nm in the center. The holes were made elliptical to give an additional design parameter to separately optimize the TE and TM mode Q factors. The elliptical hole semi-axes are 78 nm and 100 nm in the mirror section, and the hole size-to-spacing ratio is held constant through the taper section. This design yields cavity parameters of $Q = 1.4 \times 10^7$ and $V_n = 0.77$ for the TE mode, and $Q = 1.3 \times 10^5$ and $V_n = 1.44$ for the TM mode (V_n is the mode volume normalized by $(\lambda/n)^3$). The factor γ/γ_0 $= 0.10$ (0.20) for the TE (TM) mode is determined by simulating the total power emitted by a non-resonant dipole source in the cavity center. We have accounted for the index dispersion of our candidate material, GaAs, for which $n(1425 \text{ nm}) = 3.38$ and $n(950 \text{ nm}) = 3.54$ [47].

The nonlinear parameter g_2 is determined by calculating the volume integral of Eq. (3) using the exact mode fields, E_a and E_c, extracted from our 3D-FDTD calculation. Because the mode fields are oriented along the y and z-axes, respectively, as defined in Fig. 2(c), the classical field which drives the difference frequency generation, E_b, must be polarized along x. This field has a frequency $\omega_b = \omega_a - \omega_c$, which corresponds to a wavelength $\lambda_b = 2.85$ μm. The relevant nonlinear susceptibility tensor elements are $\chi_{xyz}^{(2)}(GaAs) = 2d_{14} = 550$ pm/V and $\chi_{xyz}^{(2)}(GaP) = 320$ pm/V [48, 49]. Based on previous investigations of the second-order nonlinear properties of a photonic crystal cavity [18], we expect the bulk $\chi^{(2)}$ tensor to be the relevant quantity of interest, and surface effects to play a minor role.

We assume the classical field is constant over the spatial extent of the cavity modes, which allows $E_{b,x}$ to be taken in front of the integral for g_2, giving

$$g_2 = -\frac{\varepsilon_0 E_{b,x}}{\hbar} \int d\mathbf{r} \chi_{xyz}^{(2)} E_{a,y}^* E_{c,z}. \tag{8}$$

To justify this assumption, we simulated a Gaussian beam with $\lambda_b = 2.85$ μm that is focused by a lens with a modest numerical aperture (NA) of 0.5 onto a ridge waveguide, and found that the average field amplitude is approximately uniform over the linear extent of our cavity modes (approx. $x = -1$ μm to $+1$ μm). In the g_2 calculation, the magnitude of $E_{b,x}$ for a given beam power, P_b, is then determined from the relation $P_b = \varepsilon_0 c \pi r^2 E_{b,x}^2/4$, where r is the focal spot radius.

In order to efficiently drive the difference-frequency process, the coupling field (E_b) must have a wavelength $\lambda_b = 2.85$ μm, which could be achieved using a type of Er^{3+}-doped laser [50], which can output tens of mW of cw power in the range 2.7-2.9 μm. GaAs is an attractive nonlinear cavity material because it has a reasonably large $\chi^{(2)}$ strength [48], a high refractive index, and mature microfabrication techniques.

As evident in Fig. 2, the overlap of the two modes changes sign near the edges of the ridge compared to the middle due to the different symmetries of the TE$_0$ and TM$_2$ modes. However, the induced nonlinear polarization is dominated by the negatively signed anti-nodes near the middle of the ridge, and the imperfect overlap in the integral can be completely compensated for by a stronger pump beam. Thus, by selecting a higher order TM$_2$ mode, we have gained
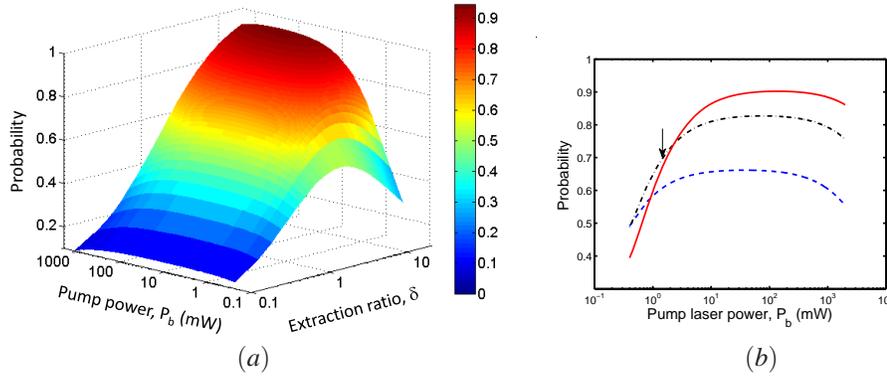
Fig. 3. Probability of single-photon frequency conversion from 950 nm to 1425 nm. The photon is coupled into a well-defined output channel at rate $\kappa_{c,ex}$. Note that the internal probability of conversion in the absence of an over-coupled extraction channel is 0.99. (a) Probability as a function of the pump laser power, P_b, and the extraction ratio, $\delta = \kappa_{c,ex}/\kappa_{c,in}$. For a given δ, there is an optimal operating power, P_b, as visible by the sharp contour ridge at small P_b. (b) Probability as a function of P_b for different values of δ. Because of the rapid rise in probability at low P_b, the system does not need to be operated at the optimum to achieve high conversion probabilities. For example, for $\delta = 10$, a probability of $F = 0.7$ can be achieved with a pump power $P_b = 1.5$ mW (indicated by the arrow).

a larger frequency conversion bandwidth at the expense of the somewhat higher pump power required to overcome the ensuing phase mismatch. For applications requiring relatively small frequency shifts, the two fundamental modes, TE_0-TM_0, would be a more appropriate choice, as their overlap is almost perfect [17].

We now calculate the probability to convert a single photon from 950 to 1425 nm in our system. The optimized cavity design simultaneously yields high quality factors and small mode volumes, which allows for extremely high cooperativities for each mode ($C_{in} > 10^4$). From Eq. (7) we find that this enables an internal conversion probability of up to $F = 0.99$ when waveguide extraction efficiency is not taken into account. In practice, to efficiently out-couple the frequency-converted single photon into a waveguide, we require the ratio $\delta = \kappa_{c,ex}/\kappa_{c,in}$ to be large (i.e. overcoupled). The branching parameter ϕ scales as $P_b/(\kappa_{c,in}(1+\delta))$, and so to increase the extraction ratio δ, the pump power (P_b) must also be increased to maintain the optimal ϕ. Essentially, achieving good extraction efficiency requires one to intentionally increase the losses in mode c (via the out-coupling waveguide), which in turn requires more pump power to maintain the critical coupling. This relationship is made clear in Fig. 3, which plots the probability F as a function of pump power P_b and extraction ratio δ. For a given δ, the power P_b can be chosen to maximize the probability, reflecting the optimal value of g_2 for frequency conversion. The probability rises rapidly with P_b, reaching a maximum at relatively low powers (visible as the sharp ridge in the contours). Three fixed δ contours are plotted in Fig. 3(b), demonstrating that efficient extraction of frequency-converted photons can be realized at modest pumping powers. For example, for $\delta = 5$, an extraction probability of 0.7 can be realized with a coupling laser power of 1.5 mW focused in a diffraction-limited focal spot. For this particular cavity design, the outgoing converted photon can be shaped to have a bandwidth of up to $\kappa_c \sim 100$ MHz.

The seemingly high power of the coupling laser (1.5 mW) is required to achieve a sufficiently high electric field amplitude (E_b) in the cavity (4.2×10^5 V/m). However, only a small fraction

of the coupling photons participate in the frequency conversion process, due to the discrepancy in size between the cavity mode and the coupling laser spot size. We have sketched a free-space, diffraction-limited coupling beam in Fig. 2 for simplicity, but if the coupling laser were coupled via the cavity waveguide, the power level required would be more than an order of magnitude smaller. Alternatively, if the difference frequency coincided with a third cavity mode, the local field enhancement in that mode would also greatly reduce the operating power. We also note that the operating power reflects in part the phase mismatch between the TE_0 and TM_2 cavity modes. Frequency conversion over smaller wavelength bands could be achieved at microwatt coupling power levels with the TE_0-TM_0 mode pair, which, as mentioned above, have an extremely high overlap function [17].

By exploiting the scaling properties of Maxwell's equations, it is straightforward to design a similar cavity in GaP, a large bandgap semiconductor which could support cavity modes at 637 nm and 950 nm. Accounting for the exact refractive index dispersion and $\chi^{(2)}$ strength of GaP, we calculate an internal frequency conversion probability on this platform of 0.99, and an extraction probability 0.7 for < 4 mW coupling power. The 637-950 nm span would be sufficient to couple any pair of the most relevant quantum emitters, namely NV centers in diamond; atoms such as Cs or Rb; and InAs/GaAs quantum dots. Such a cavity could also be integral to creating a stable, room temperature single-photon source emitting in the telecom band based on frequency-converted NV center emission in diamond [51]. Given the challenge of fabricating high-Q cavities directly in diamond [52], hybrid approaches involving GaP-diamond heterostructures [53, 54, 55, 56] or diamond nanocrystals [57, 58] are promising alternatives to realize cavity-coupled NV center emission. We have shown previously that, despite a small perturbation of the cavity, the strong coupling regime can still be accessed with a diamond nanocrystal positioned on top of a photonic crystal nanobeam cavity [37]. Given that it may be difficult to span the large spectrum from 637 nm to telecom wavelengths in a single monolithic design, a 637-950 nm cavity could be the first stage of a two-step frequency conversion process involving our first example as the second stage. More generally, cascading allows our design to be extended to cover virtually any frequency span.

5. Summary and outlook

We have shown that high-efficiency, intra-cavity frequency conversion of single photons from a dipole-like emitter can be achieved using a two-mode nonlinear cavity pumped by a classical field. Our general framework is valid for conversion between arbitrary frequencies, and the efficiency depends only on the cavity parameter Q/V. Further design improvements should lead to larger frequency spans and also lower pump power requirements (*e.g.*, by allowing ω_b to correspond to a third cavity mode). Although we have emphasized large frequency shifts in this paper, a smaller shift could be readily achieved by coupling the TE_0 mode with the fundamental TM_0 mode, which has a larger Q factor than the TM_2 mode studied here. The TE_0-TM_0 modes have a larger spatial overlap, reducing the coupling power required for high probability frequency conversion. In our scheme, wavelength trimming to achieve the strong coupling condition between the cavity and emitter could be readily achieved by temperature or electrostatic tuning [59, 60], and additional dynamical tuning functionality could potentially be realized by optomechanical effects [42].

Beyond the aforementioned applications, the techniques described here can potentially be extended to open up many intriguing opportunities. For example, the photon emission of a particular emitter could be shifted into wavelengths where high-efficiency detectors are available. It also allows coupling of atomic emitters such as Cs or Rb with solid-state emitters to create hybrid atom-photonic chips [61]. In addition, a number of quantum entanglement schemes for atoms rely on joint photon emission and subsequent detection to probabilistically project the

atomic system into an entangled state [62, 63, 64]. Such schemes rely on the indistinguishability of photons emitted from each atom, and implementing such techniques in nonlinear cavities could allow entanglement between different types of emitters. In addition, the protocol described here could be extended for generating narrow-bandwidth, entangled photon pairs with high efficiency and repetition rates, which are a valuable resource for applications such as quantum cryptography [65]. Our scheme could also be applicable in active materials, where laser wavelengths could be converted from easily accessible regions like 1500 nm to the mid-infrared range.

Appendix

Derivation of nonlinear conversion efficiency

The state amplitudes of the wave-function given in Eq. (4) evolve under the interaction Hamiltonian H_I of Eq. (1) through the following equations,

$$
\begin{aligned}
\dot{c}_s &= -i\Omega(t)c_e, \\
\dot{c}_e &= -i\Omega(t)c_s - ig_1 c_a - (\gamma/2)c_e, \\
\dot{c}_a &= -ig_1 c_e - ig_2 c_c - (\kappa_a/2)c_a, \\
\dot{c}_c &= -ig_2 c_a - (\kappa_c/2)c_c.
\end{aligned}
\tag{9}
$$

These equations describe both coherent evolution (terms proportional to $\Omega(t), g_{1,2}$) and population loss in the system (terms proportional to $\gamma, \kappa_{a,c}$). The population loss in the system can be connected to direct radiative emission of the excited state $|e\rangle$ (at a rate $\gamma|c_e|^2$), radiation leakage and absorption losses of mode a ($\kappa_a|c_a|^2$), and absorption and leakage out of mode c ($\kappa_c|c_c|^2$, of which $\kappa_{c,ex}|c_c|^2$ is successfully out-coupled to a waveguide). In general the efficiency of extracting a single photon of frequency ω_c out into the waveguide is thus

$$
F = \frac{\int_0^\infty dt\, \kappa_{c,ex}|c_c(t)|^2}{\int_0^\infty dt\, \kappa_c|c_c(t)|^2 + \kappa_a|c_a(t)|^2 + \gamma|c_e(t)|^2}.
\tag{10}
$$

For arbitrary $\Omega(t)$, Eqs. (9) and (10) can be evaluated numerically. However, in certain limits one can find approximate solutions. In particular, when $\Omega(t)$ and its rate of change are small compared to the natural oscillation and decay rates of the system, the state amplitudes $c_{a,c,e}$ will follow the instantaneous value of $c_s(t)$. Formally, we can adiabatically eliminate these states, setting $\dot{c}_i = 0$ for $i = a, c, e$. Then, one finds

$$
\dot{c}_s(t) = -\frac{2\Omega(t)^2}{\gamma_{\text{total}}}c_s(t),
\tag{11}
$$

while the other $c_i \propto c_s(t)$, with the proportionality coefficients being functions of $g_1, g_2, \kappa_a, \kappa_c, \Omega(t)$. The resulting substitution of the solutions of $c_i(t)$ into Eq. (10) allows great simplification because the integrands now become time-independent, and after some simplification yields Eq. (6). Self-consistency of the adiabatic elimination solution requires that the the effective rate of population loss $\sim 4\Omega(t)^2/\gamma_{\text{total}}$ predicted from state $|s\rangle$ does not exceed the rate κ_c that a photon can leak out through the cavity mode c.

In the effective wave-function approach used here, the population leakage out of mode c can also be explicitly related to the shape of the outgoing single-photon wavepacket. For instance, we can model the linear coupling of cavity mode c to photons propagating in a single direction in a waveguide with the following Hamiltonian (in a rotating frame),

$$
H_w = \int dk\, \hbar v(k - \omega_c/v)\hat{a}_k^\dagger \hat{a}_k - \hbar g_w \int dk \left(\hat{a}_c^\dagger \hat{a}_k e^{ikz_c} + h.c. \right).
\tag{12}
$$

Here k denotes the set of wavevectors of the continuum of waveguide modes, v is the velocity of waveguide fields, g_w is the coupling strength between cavity and waveguide modes, and z_c denotes the position along the waveguide where the cavity is coupled to it (for simplicity we set $z_c = 0$ from this point on). Since we are now explicitly accounting for the waveguide degrees of freedom, we add a term $\int dk\, c_k(t)|1_k\rangle$ to the effective wave-function of the system. The equations of motion of the total system are identical to Eq. (9), except that

$$\dot{c}_c = -ig_2 c_a - (\kappa_{c,in}/2)c_c + ig_w \int dk\, c_k, \tag{13}$$

$$\dot{c}_k = -iv(\delta k)c_k + ig_w c_c, \tag{14}$$

where $\delta k = k - \omega_c/v$. Compared to Eq. (9), we have now included the coupling of mode c to the waveguide, and accordingly have replaced $\kappa_c \to \kappa_{c,in}$ in the equation for $\dot{c}_c$ since the leakage into the waveguide should be accounted for by the new coupling terms. The equation for $\dot{c}_k$ can be formally integrated; assuming that the waveguide initially is unoccupied, $c_k(0) = 0$, one has

$$c_k(t) = ig_w \int_0^t dt'\, c_c(t')e^{-ic\delta k(t-t')}. \tag{15}$$

Substituting this into the equation for $\dot{c}_c$ and performing the Wigner-Weisskopf approximation [66], one recovers the expression for $\dot{c}_c$ in Eq. (9) by identifying $\kappa_{c,ex} = 2\pi g_w^2/v$. The one-photon wave-function [66] is given by $\psi_w(z,t) = \langle vac|\hat{E}_w(z,t)|\psi(0)\rangle = (\sqrt{2\pi}ig_w/v)\Theta(z)c_c(t - z/v)$, where $\Theta(z)$ is the step function. The wave-function shape is thus directly proportional to $c_c(t)$. Under adiabatic elimination,

$$\psi_w(z,t) = \frac{\sqrt{2\pi}ig_w}{v}\Theta(z)\frac{8ig_1g_2}{\gamma_{total}(\kappa_a\kappa_c + 4g_2^2)}\Omega(t - z/v)c_s(t - z/v), \tag{16}$$

and thus for a desired (and properly normalized) pulse shape ψ_w one needs only to solve Eqs. (16) and (11) to obtain the corresponding external field $\Omega(t)$. It is straightforward to show that the normalization is given by $\int dz\,|\psi_w(z,t\to\infty)|^2 = F$ provided that $c_s(\infty)\to 0$. This normalization reflects the probability that a single photon ends up in the waveguide.

Dephasing

We now consider the effects of dephasing on our previous analysis. In the presence of dephasing, it is necessary to solve for the full density matrix ρ of the system, whose evolution is given by $\dot{\rho} = -(i/\hbar)[H_c,\rho] + L[\rho]$. Here H_c is the Hamiltonian describing the coherent evolution, and $L[\rho]$ is the Liouvillian describing the decoherence and dissipative processes,

$$L[\rho] = -\sum_{j=a,c}\frac{\kappa_j}{2}\left(a_j^\dagger a_j\rho + \rho a_j^\dagger a_j - 2a_j\rho a_j^\dagger\right) - \frac{\gamma}{2}(\sigma_{ee}\rho + \rho\sigma_{ee} - 2\sigma_{ge}\rho\sigma_{eg})$$

$$\qquad - \frac{\gamma_d}{2}(\sigma_{ee}\rho + \rho\sigma_{ee} - 2\sigma_{ee}\rho\sigma_{ee}), \tag{17}$$

where γ_d describes the pure dephasing of the excited state.

The full density matrix equations in principle can be adiabatically eliminated as before, but the general solutions are quite cumbersome and offer little insight. To simplify the situation, we assume that cavity mode c can be effectively eliminated to yield a new effective linewidth $\kappa_a \to \kappa_a(1 + \phi)$ for cavity mode a, and from this point forward consider the reduced system consisting of states $e, g,$ and a. We then adiabatically eliminate the density matrix elements for this system in terms of ρ_{ss}. Of particular interest here are the equation of motion for the

population ρ_{ss} in the meta-stable state, the population of the cavity mode ρ_{aa}, and the coherence ρ_{as} in the limit of weak driving (Ω small),

$$\dot{\rho}_{ss} \approx -\frac{4\Omega^2(1+\phi)}{(\gamma+\gamma_d)(1+\phi)+C_{in}\gamma}\rho_{ss}, \tag{18}$$

$$\rho_{as} \approx -\frac{4g_1\Omega}{4g_1^2+(\gamma+\gamma_d)(1+\phi)\kappa_a}\rho_{ss}, \tag{19}$$

$$\rho_{aa} \approx \frac{4C_{in}\Omega^2(\gamma+\kappa_a(1+\phi))}{\kappa_a((\gamma+\gamma_d)(1+\phi)+C_{in}\gamma)(\gamma(1+\phi)+(C_{in}+1+\phi)(\gamma+\kappa_a(1+\phi)))}\rho_{ss}. \tag{20}$$

We now derive the probability that the excitation initially stored in state s decays through cavity mode a. This probability is given by

$$\frac{\kappa_a(1+\phi)\rho_{aa}}{\dot{\rho}_{ss}} = \frac{C_{in}(\gamma+\kappa_a(1+\phi))}{\gamma_d(1+\phi)+(C_{in}+\phi+1)(\gamma+\kappa_a(1+\phi))}. \tag{21}$$

In the presence of dephasing, the expression above should replace the first term on the right-hand side of Eq. 6, leading to a reduction in the single-photon conversion efficiency. In particular, note that this quantity simplifies to $\frac{C_{in}}{C_{in}+\phi+1}$ in the limit that $\gamma_d \rightarrow 0$. A second relevant quantity to consider is the *coherence* of the generated single photon. Specifically, in the ideal process (with $\gamma_d = 0$) a definite phase relationship is established between the outgoing photon and the state s. Maintaining coherence is important in the ability to create indistinguishable photons over successive operations of the device, or being able to implement the time-reversal of the generation process (*i.e.*, coherent photon storage). We define the coherence by $\mathscr{C} \equiv |\rho_{as}|^2/\rho_{aa}\rho_{ss}$, which for our system is given by

$$\mathscr{C} = \frac{\gamma(\gamma_d(1+\phi)+(C_{in}+1+\phi)(\gamma+\kappa_a(1+\phi)))}{((\gamma+\gamma_d)(1+\phi)+\gamma C_{in})(\gamma+\kappa_a(1+\phi))}. \tag{22}$$

Note that for $\gamma_d \rightarrow 0$, the coherence reaches its maximum allowed value of $\mathscr{C} = 1$.

Acknowledgements